

The Structure of Synchronization Sets for Noninvertible Systems

Krešimir Josić and Evelyn Sander

October 17, 2003

Abstract

Unidirectionally coupled systems $(x, y) \mapsto (f(x), g(x, y))$ occur both naturally, and are used as tractable models of models with complex interactions. We analyze the structure and bifurcations of the attractor in the case the driving system is not invertible, and the response system is dissipative. We discuss both cases in which the driving system is a map, and a strongly dissipative flow. Although this problem was originally motivated by examples of nonlinear synchrony, we show that the ideas presented can be used more generally to study the structure of attractors, and examine interactions between systems in networks.

Synchronization in networks of systems with complex behavior has been a topic of extensive experimental and theoretical study in recent years [6, 22, 29]. Roughly, a network is synchronized when there is a relationship between the dynamics of its constituent systems, so that information about one system can be gained by observing the behavior of another system in the network. More formally, a network exhibits generalized synchrony if the attractor of the network is contained within a *synchronization set* with a certain structure [7, 25]. In many cases, the synchronization set is the graph of a smooth map. However, a network may still be synchronized even when its synchronization set is more complicated. In this paper, we consider the case in which the synchronization set is the graph of multiple curves as result of noninvertibility of systems within the network [2, 5, 23, 27]. We provide a mathematical justification of many claims made in our earlier paper [5]. In addition, we extend the work by studying the implications of results obtained for noninvertible maps to flows, analyzing the bifurcations leading to the complicated structures we observe, and explaining how these observations carry over to higher dimensional maps. In this context we also give an explanation of a synchronization detection technique which was recently introduced by He, Zhang and Stone [13], and answer an open problem posed by Afraimovich, et al. [2].

1 Introduction

A class of models frequently used in the study of synchrony are unidirectionally coupled systems,

$$(x, y) \mapsto (f(x), g(x, y)), \quad (1.1)$$

also known as drive-response, or skew product systems. When the driving map $x \mapsto f(x)$ is invertible, it is known that for sufficiently strong coupling the synchronization set is the graph of a smooth function $\phi : X \rightarrow Y$ from the drive space X to the response space Y (see Section 3 and [16] for a precise statement).

In many important cases the driving system $x \mapsto f(x)$ is noninvertible. This can occur if the driving system is obtained by reconstruction and the sampling dimension is too small, if a stroboscopic equation for a differential equation is sampled too infrequently [10], or as a result of inherent noninvertibility, as in delay equations or numerical approximations [18]. It has recently been observed that in such situations the synchronization set may lose the structure of a smooth manifold, hampering traditional detection methods [2, 5, 23, 13].

A synchronization set with a structure typical of such examples is shown in Fig. 1, and is discussed in Section 2. In this case the synchronization set has the structure of the image of a Cantor set of lines in the vicinity of most points. We will show that such structures can be generally expected when the drive is noninvertible, although the local geometry is typically even more complex. Similar structures can be observed in higher dimensional maps, as well as flows which project to noninvertible maps along strong stable foliations. We note that the synchronization set can be multivalued even for invertible maps, although in this case the structure of the synchronization set is very different [24].

In this paper we discuss the structure and bifurcations of synchronization sets in the presence of noninvertible drives, including representative examples illustrating the types of possible behavior. The paper proceeds as follows: In Section 2 we present a number of examples of multivalued synchronization sets in networks with noninvertible drives and bifurcations that lead to such attractors. In Section 3, we indicate how to extend the standard proofs which work for invertible systems to show the existence and continuity of synchronization sets in the present case. In Section 4, we use a constructive approach to show continuity. This has the advantage of giving more detailed structural information, which is illustrated in several simple examples. The synchronization set may be the union of graphs of uncountable or countable number of continuous functions. We give an example of a synchronization set comprised of a countable number of graphs when the drive has positive topological entropy, answering a question posed in [2], and show that in pathological cases, the synchronization set can lose the structure of a union of curves. In Sections 4.5 and 4.6, we use inverse limit techniques to establish the validity of the ϵ - δ^p method for the detection of generalized synchrony for systems with noninvertible driving maps described in [13]. Section 5 revisits the examples from Section 2.3, giving a proof that typically the synchronization set is nearly smooth and non-intersecting near the bifurcation to a noninvertible drive. In Section 6, we give an alternative construction for synchronization sets which can be used to prove smoothness of individual curves within the family.

To avoid introducing burdensome notation into the examples and arguments we primarily discuss noninvertible systems in one dimension. Most of the arguments can be extended to higher dimensional systems in a straightforward way.

2 Examples of Networks with Noninvertible Drives

In this section we consider examples of drive-response system that illustrate the typical phenomena that can be expected in such systems. The general ideas illustrated in these examples will be studied in subsequent sections.

2.1 Unimodal Maps of the Interval

The simplest example of noninvertible drive in a system of the form of Equation 1.1 is one for which the drive is a tent map:

$$f(x) = \begin{cases} cx & \text{if } x \in [0, 1/2) \\ -cx + c & \text{if } x \in [1/2, 1]. \end{cases} \quad (2.2)$$

where $c \in (0, 2]$. As long as the response $g(x, y)$ is contracting in the second variable, the attractor of the network (x, y) will be contained in a collection of lines which are connected along the forward orbit of the critical point. If $c = 2$ the forward orbit of the critical point is $(\{1/2, 1, 0, 0, \dots\})$. Since this orbit is finite the vertical line $x = \text{const.}$ intersects this collection in a Cantor set of points in most places. The different lines in this collection are joined along “hooks” that occur above the forward orbit of the critical point, and may intersect at other points. This situation is illustrated in Fig. 1a and b with $g(x, y) = dy + x^2$, $d = 0.3$, and $c \approx 2$. (See remark 4.5 for a comment on the numerical implementation.)

The orbit of the critical point is in general not finite for unimodal maps and may be dense in $[0, 1]$. In such situation, the “hooks” may appear densely throughout the synchronization set. Using visual inspection the cases of finite and infinite critical orbits appear similar. Fig. 1c was obtained by using (2.2) as a drive, with response $g(x, y) = ky + \sin(2\pi x)$, and $c = 1.9$ and $k = 0.5$. In this case, the orbit of the critical point does not have a low period. The synchronization set appears to be a set of curves, however the magnification shown in Figure 1d shows that “hooks” appear throughout the synchronization set, over the forward orbit of the critical point. In the case the forward orbit of the critical point is dense, under repeated magnification one would see that “hooks” occur arbitrarily close to any point in the synchronization set. This structure is further explained in Section 4.

2.2 Drives with strong stable foliations

The synchronization set can have a similar structure for strongly dissipative flows. The attractors for such flows frequently possess strong stable foliations along which the dynamics project to lower dimensional noninvertible maps. The Lorenz system in the standard chaotic regime ($\sigma = 10, \rho = 28.0, \beta = 8/3$) has this property. The Poincaré Map taken at $z = 27$ has

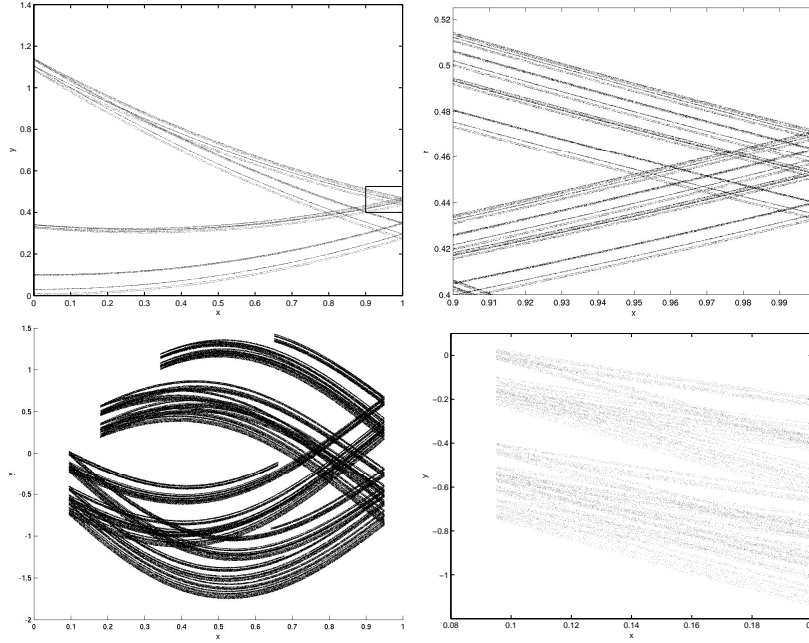


Figure 1: a. (left) The synchronization set for a drive-response system in which f is the tent map. b. (right) A blowup of the square in the a shows the rich Cantor-like structure of the attractor. c. (top left) The synchronization set for a drive-response system in which f is the tent sine map described in the text, and the orbit of the critical point is finite. d. (top right) A blowup of the square in c.

an attractor with a strong stable foliation along which the system projects to a noninvertible map of the interval [11, 30]. If such a system is used as a drive the synchronization set can display the structure shown in the previous example.

Consider the Lorenz system $x' = \sigma(y - x), y' = \rho x - y - xz, z' = -\beta z + xy$ driving the system $r' = -cr + x$. The fibers $(x, y, z) = \text{const.}$ are contracted under the flow of this system, and the intersection of its attractor with the hyperplane $z = 27$ has a local structure that resembles a Cantor set of lines (see Fig. 2). Similar results can be obtained by using any combination of the x and y variable to drive a response system that is uniformly contracting.

As will be shown in Section 6 we can think of figure 2b as a nonlinear magnification of the intersection of the Lorenz attractor with the Poincaré surface $z = 27$. Due to the high rate of contraction, the fractal structure of the Lorenz attractor is hard to resolve on the surface $z = 27$, and the intersection of the attractor with this section appears as four lines. As shown in Fig. 2 under “magnification” these lines are resolved to what appears to be a Cantor set of lines. Lorenz already noted that, although the attractor appears to be a surface due to high dissipation, it has to have a complicated transversal structure [17].

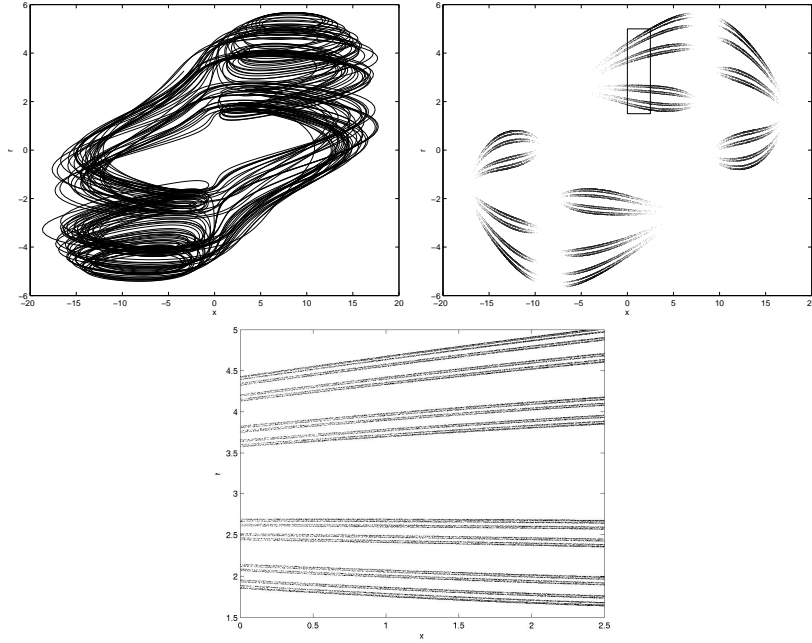


Figure 2: a. (left) Lorenz system driving a linear response $r' = -cr + x$. The upper left figure gives the projection of the attractor from $\mathbb{R}^3 \times \mathbb{R}$ onto the x and r variables. b. (upper right) The section $z = 27$ of the attractor on the left. c. (lower) A blowup of the square in b shows the Cantor-like structure in this example.

It is this structure that becomes apparent after magnification. These observations are not affected by small noise, and could therefore be useful in studying the attractors of highly dissipative systems from experimental data.

The Rössler attractor also appears to have a similar strong stable foliation, and if used as a drive in $x' = -y - z, y' = x + 0.15y, z' = zx - 10z + 0.2, r' = -cr + x$ with $c = 0.2$, we obtain the attractor shown in Figure 3. As the Poincaré Map looks like a “fattened” unimodal map, the structure of the attractor in this section appears as a collection of lines joined along the forward orbit of the critical point of this map. Note the similarity between this attractor and that in Fig. 1. A response to two different response system are shown in Figs. 1c and 1d. Although the Poincaré Map $y = 0$ of the attractors look different, the “hooks” still have the same x, z coordinates.

2.3 The onset of noninvertibility

In this section we illustrate the transition from a synchronization set contained in the graph of an interval (as the result of an invertible drive) to one which is contained in the graph of a multivalued function (as the result of a noninvertible drive). Two types of transitions

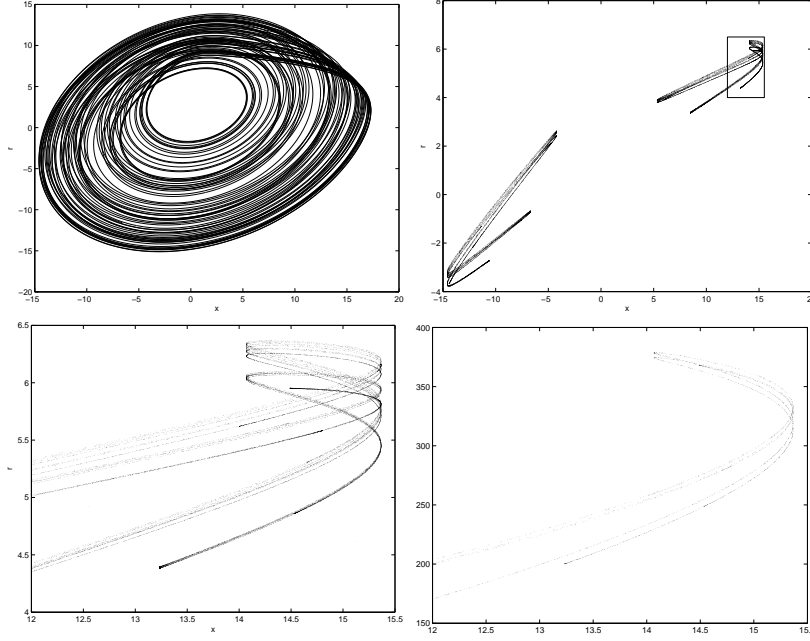


Figure 3: a. (upper left) A projection of attractor of Rössler system used as a drive with response $r' = -cr + x$, $c = 0.2$. from $\mathbb{R}^3 \times \mathbb{R}$ onto the $x-r$ plane. b. (upper right) Projection of the section $y = 0$ of the attractor on the left. c. (lower left) A blowup of the square in b shows the Cantor-like structure in this example. d. (lower right) A blowup of the attractor of the same drive and response $r' = -cr + x + y^2$, with $c = 0.2$.

are illustrated in Fig. 4. Also see URL [26] for an animated version of this figure.

Following [5] we introduce a two-parameter family of drive-response systems:

$$\begin{aligned}
 u_{n+1} &= \begin{cases} \lambda\omega(u_n, s, \rho) & v_n < \alpha \\ \lambda + (1 - \lambda)u_n & v_n \geq \alpha \end{cases} \\
 v_{n+1} &= \begin{cases} v_n/\alpha & v_n < \alpha \\ (v_n - \alpha)/(1 - \alpha) & v_n \geq \alpha \end{cases} \\
 y_{n+1} &= cy_n + \cos(2\pi u_{n+1})
 \end{aligned} \tag{2.3}$$

where $(u, v) \in [0, 1] \times [0, 1]$, $0 < \lambda < 1$ and $0 < \alpha < 1$, $1 > c \geq 0$, while s and ρ are parameters which will be varied. The (u, v) subsystem, which serves as the drive, is a generalized baker's map. The lower portion of the square is mapped by $\omega(u, s, \rho)$, a function of u depending on the parameters s and ρ .

In [5] a one parameter family $\omega(u, s, \rho) = \omega(u, s) : [0, 1] \rightarrow [0, 1]$ of cubic functions determined by the conditions $\omega(0, s) = 0, \omega(1/2, s) = 1/2, \omega(1, s) = 1$, and $\frac{d\omega}{du}(1/2, s) = s$ was used to illustrate this bifurcation (see Fig.5b). For parameter $s > 0$, the function is invertible, and the synchronization set is the graph of a smooth function (see Fig. 4a). The

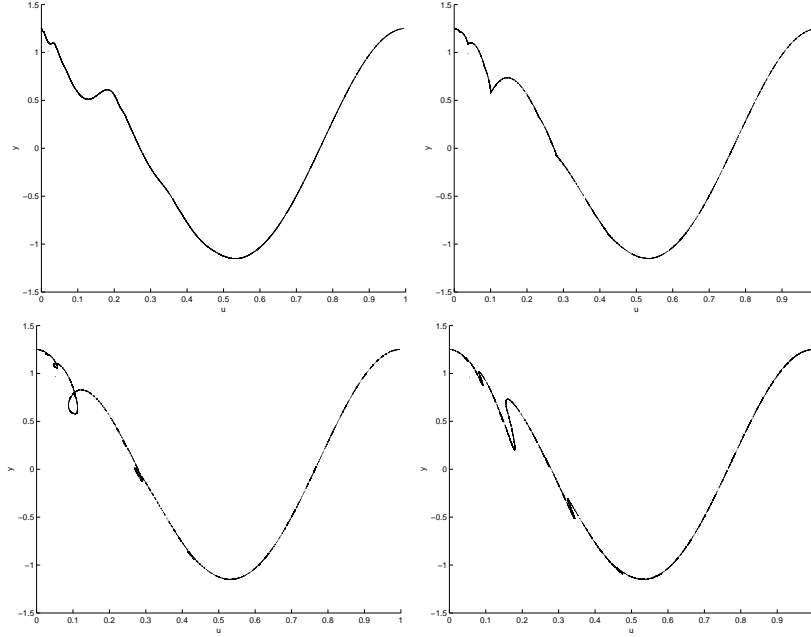


Figure 4: The attractor of system (2.3). a. (upper left) When the driving map is invertible, the synchronization set is smooth. b. (upper right) In special cases, at the onset of noninvertibility the synchronization set appears to develop cusps. c. (lower left) As the driving system becomes noninvertible loops are formed. d. (lower right) In a typical transition, places with vertical tangents transition to “bends” in the graph, and no loops appear.

attracting set of system (2.3) is constant in the v direction, and it is therefore sufficient to plot its projection onto the $u - y$ plane. At $s = 0$, the function ω has a critical point (an inflection point) at $u = 1/2$. As a result, cusps seem to develop in the synchronization set which thereby loses smoothness (see Fig. 4b). When $s < 0$, ω_s is noninvertible, the cusps immediately transform to self-intersecting loops (see Fig. 4c). Note that the synchronization set is not a smooth manifold at the bifurcation point $s = 0$, and ceases to be a manifold after the bifurcation. In a certain sense, this transition corresponds to a bifurcation of codimension 2, and is therefore atypical.

In Figure 4c, notice that at $u \approx 1/2$, the synchronization set has a critical point, the same point at which ω has a critical point. The coincidence of the critical point of the invariant graph and the function ω causes the cusps and the loops.

This simultaneity of the principal critical points is not typical for one-parameter families functions. In the typical case, the invariant graph will transition to a smooth, non-self intersecting curve, without the appearance of cusps and loops. If there are no cusps, then after the onset of noninvertibility the synchronization set continues to be non-self intersecting and close to a smooth manifold, although it is no longer the graph of a map. See Figure 4d.

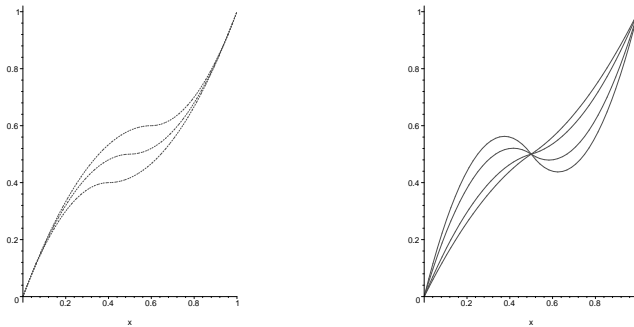


Figure 5: Graph of $\omega(u, s, \rho)$. a. (left) Parameter ρ determines the location of the critical fixed point. Values $\rho = 0.4, 0.5$, and 0.6 are shown. b. (right) Parameter s determines the slope at the critical fixed point. Values $s = -0.5, 0.2$, and 0.5 , with $\rho = 0.5$ are shown.

To illustrate this, we introduce a parameter ρ , so that the fixed points of $\omega(u, s, \rho)$ are located at $0, \rho$, and 1 , and such that $\frac{d\omega}{du}(\rho, s, \rho) = s$. Changing ρ moves the critical point of ω away from the critical point of the invariant graph (the original map corresponds with the modified function with $\rho = 1/2$.) As shown in Fig. 5, this results in a transition to a smooth manifold. Cusps occur as a codimension two set in a three-parameter version of this family; specifically, for every c near zero, there is a (s, ρ) pair for which the system has a cusp.

3 An inverse limit approach

We consider the existence of invariant graphs in systems of the form

$$\begin{aligned} x_{n+1} &= f(x_n) & f : X &\rightarrow X \\ y_{n+1} &= g(x_n, y_n) & g : X \times Y &\rightarrow Y \end{aligned} \tag{3.4}$$

where X and Y are smooth manifolds possibly with boundary, X is compact, and f and g are continuous but not necessarily invertible. A graph of a function $\phi : X \rightarrow Y$ is invariant if $g(x_0, \phi(x_0)) = \phi(f(x_0))$, *i.e.* any point starting on the graph remains on the graph under the evolution of (3.4).

The graph transform method, which is typically used in proving the existence of invariant graphs, relies on the assumption that f is invertible [9, 15, 28], but it can be extended directly to system (3.4) by considering the inverse limit of X with bonding map f . The inverse limit space (X, f) consists of all sequences $\{x_0, x_1, x_2, \dots\}$ such that $f(x_i) = x_{i-1}$ for $i > 0$ (cf.[21, 4] for more details on inverse limits.) The map f induces a map $\hat{f} : (X, f) \rightarrow (X, f)$ defined by $\hat{f}(x_0, x_1, x_2, \dots) = (f(x_0), x_0, x_1, \dots)$. Consider the system

$$\begin{aligned} \hat{x}_{n+1} &= \hat{f}(\hat{x}_n) \\ y_{n+1} &= g(\pi_0(\hat{x}_n), y_n) \end{aligned} \tag{3.5}$$

where $\pi_0 : X \times X \times \dots \rightarrow X$ is the projection onto the first coordinate in the inverse limit space. Note that only the driving systems differ between systems (3.4) and (3.5) since the dynamics of the response remain unchanged.

The graph transform method can be applied to system (3.5), if there exists a $1 > c_1 > 0$ such that

$$d(g(\hat{x}, y_a), g(\hat{x}, y_b)) \leq c_1 d(y_a, y_b) \quad (3.6)$$

for all $\hat{x} \in X$ and all $y_a, y_b \in Y$, *i.e.* the system (3.4) contracts the fibers $\hat{x} = \text{const}$. Assume that there exists a $c_2 > 0$ which gives a limit of the contraction in the driving system, *i.e.*

$$d(\hat{f}^{-1}(\hat{x}_a), \hat{f}^{-1}(\hat{x}_b)) \leq c_2 d(\hat{x}_a, \hat{x}_b) \quad (3.7)$$

for all $\hat{x}_a, \hat{x}_b \in (X, f)$. Assuming that g and \hat{f} are smooth functions, we have the following theorem

Theorem 3.1 ([9],[15]) *Under the above assumptions there exists a bounded continuous function $\Phi : (X, f) \rightarrow Y$ such that the graph of Φ is invariant under (\hat{f}, g) and attracting for all $(\hat{x}, y) \in (X, f) \times Y$. If $c_1 c_2 < 1$ then this graph is a differentiable manifold.*

Variants of this theorem can be proved in cases f is piecewise differentiable, or only Hölder continuous [1].

4 The Structure of Invariant Collections of Graphs

Theorem 3.1 implies that, under appropriate conditions, there exists an attracting invariant graph over the inverse limit space of the driving map when the drive is noninvertible. The synchronization set lies in the projection of this graph onto $X \times Y$. The inverse limit space usually has a rather complicated structure [3, 20], which will be inherited by the invariant graph of (3.4). It is our goal to use a somewhat more direct construction to describe certain features and bifurcations of the attractor of this system. To do this we will define collections of graphs over sequences of intervals, the union of which will equal the projection of the invariant graph in Theorem 3.1.

To avoid burdensome technicalities which would be necessary in the general case, we illustrate how the attractor of system (3.4) lies in an “invariant collection of graphs” in the case the drive function f is a tent map. Next, we point out how to generalize the construction to Markov maps. A related construction is considered in [2]. In the case of non-Markov maps, an additional step is necessary in the construction, but the essential ideas remain the same. Most ideas presented in this section carry over to dynamics in \mathbb{R}^{n+1} .

4.1 Trees and branches

Assume that $g : \mathbb{R}^2 \rightarrow \mathbb{R}$ satisfies condition (3.6), and let f be the tent map (2.2) with $c = 2$.

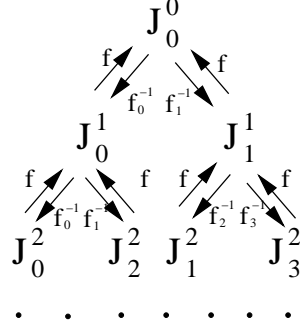


Figure 6: A tree of intervals for the map (2.2).

Consider the collection of intervals $J_k^n = [k2^{-n}, (k+1)2^{-n}]$ with $0 \leq k < 2^n$. Note that $f(J_k^{n+1}) = f(J_{2^n-k}^{n+1}) = J_k^n$ and that both maps are invertible when restricted to the intervals $J_{2^n-k}^{n+1}$ and J_k^{n+1} . Therefore the intervals J_k^n form a tree, so that f maps any interval in the tree to one in the level directly above it, and f is invertible along the branches of the tree. The inverses of f mapping J_k^n to J_k^{n+1} and $J_{2^n-k}^{n+1}$ will be denoted by f_{n+1}^{-1} and $f_{2^n-k}^{-1}$ (see Fig. 4.1).

Let $a = (a_0, a_1, \dots)$ be a sequence of integers such that $0 \leq a_i < 2^i$ so that $J_a = (J_{a_0}^0, J_{a_1}^1, J_{a_2}^2, \dots)$ is a fixed path in this tree, and let

$$G_a = \cup_{a_i} \{ \Psi_{a_i}^i \mid \Psi_{a_i}^i : J_{a_i}^i \rightarrow \mathbb{R}, \Psi_{a_i}^i \in C(J_{a_i}^i), \text{ and } \exists B \text{ such that } \Psi_{a_i}^i < B \text{ for all } i \}$$

be the collection of all sequences of bounded, continuous functions, each of which map an interval in J_a into \mathbb{R} . We can define the distance between $\Phi_a, \Psi_a \in G_a$ by

$$\bar{d}_\eta(\Phi_a, \Psi_a) = \sum_{i=0}^{\infty} \frac{d_i(\Phi_{a_i}^i, \Psi_{a_i}^i)}{e^{\eta^i}}$$

where $\eta > 0$, and d_i is the metric induced by the supremum norm in $C(J_{a_i}^i)$.

Definition 4.1 *The sequence Ψ_a is invariant under (3.4) if the graph of $\Psi_{a_{i+1}}^{i+1}$ is mapped onto the graph of $\Psi_{a_i}^i$ for $i = 0, 1, \dots$. More precisely*

$$\Psi_{a_i}^i(f(x)) = g(x, \Psi_{a_{i+1}}^{i+1}(x)) \tag{4.8}$$

for all x on which $\Psi_{a_{i+1}}^{i+1}$ is defined.

Finally let S be the set of all integer sequences $a = (a_0, a_1, \dots)$ with $0 \leq a_i < 2^i$, and let $G = \cup_{a \in S} G_a$ the collections of graphs over the intervals in the entire tree. An element $\Psi \in G$ is a collection of graphs over each possible path in the tree of intervals. Thus we have three levels at which we can view the collection of maps defined on the tree of intervals: the individual maps $\Psi_{a_i}^i$, sequences of maps Ψ_a and collections of sequences Ψ .

4.2 The synchronization set

In this section, we illustrate the proof of the following:

Theorem 4.2 *For a system of the form (3.4), where f is continuous piecewise monotone map of the interval with all critical points having finite forward orbits, and g satisfies condition (3.6), the synchronization set is contained in a collection of continuous graphs.*

Since f is a Markov map, there exists a tree structure analogous to the one described in the previous section, and the synchronization set is a collection of continuous graphs over the intervals that occur as branches in the tree. This sequence is obtained as an invariant element in G .

The proof is a straightforward generalization of the graph transform method to graphs defined over sequences of intervals. We first assume that f is a tent map, and then show that a similar argument works in the general case. The statement is proved by defining a map $\Gamma_a : G_a \rightarrow G_a$ which is a contraction, and whose fixed point is the desired graph.

The graph transform is defined as

$$\Gamma_{a_i}(\Psi_{a_i}^i)(x) = g(f_{a_{i+1}}(x), \Psi_{a_{i+1}}^{i+1}(f_{a_{i+1}}^{-1}(x)))$$

Following the construction above, the map $\Gamma_a = (\Gamma_{a_0}, \Gamma_{a_1}, \dots)$ is defined to act on sequences of graphs. It is straightforward to check that a fixed point of the map Γ_a satisfies (4.8), and maps G_a into itself. It remains to check that the map is a contraction, to show the existence of a fixed point Ψ_a^* . This is done in the Appendix.

The argument is independent of the sequence a chosen in the construction. Therefore the union of all invariant graphs $\cup_{a \in S} \Psi_a^*$ forms an invariant collection of graphs Ψ^* . Under the dynamics of the system graphs over one level in the tree get mapped to graphs at the next level. Each sequence Ψ_a^* terminates in the top level graph $\Psi_{a_0}^{0*}$. To see where the top level graph is mapped to, note that it is a union of two graphs $\Psi_{b_1}^{1*}$ and $\Psi_{c_1}^{1*}$ where the sequences b and c are defined by $b = (b_0, b_1, b_2, \dots) = (0, 0, a_1, a_2, \dots)$ and $c = (c_0, c_1, c_2, \dots) = (0, 1, a_1, a_2, \dots)$, so that the image of $\Psi_{a_0}^{0*}$ must be $\Psi_{b_0}^{0*} \cup \Psi_{c_0}^{0*}$.

By the same argument, the collection of all 2^k graphs that share the same terminating sequence a , but have different initial sequences, *i.e.* all graphs corresponding to sequences of the form $(0, \underbrace{\dots, \dots}_k, a_1, a_2, \dots)$ form the graph corresponding to the sequence $a = (0, a_1, a_2, \dots)$.

This argument can be used directly to explain the structure of the synchronization set in Fig. 1a and b where f is given by (2.2) map and $g(x, y) = dy + x^2$. The attractor is contained in a collection of graphs from $[0, 1]$ to \mathbf{R} . Each of the graphs in this collection is mapped to two graphs connected at $x = 1$. Fig. 7 illustrates this by showing the first three iterates of the unit square. The attractor of system (3.4) is contained in the collection of graphs Ψ , although it is typically only a proper subset.

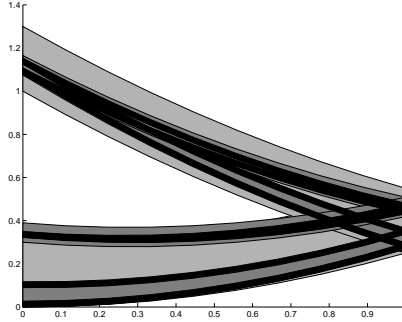


Figure 7: The light gray, dark gray, and black regions represent respectively the first, second and third iterates of the unit square under the evolution of the drive-response system described in the text (compare with Fig. 1a and b.)

If f is a piecewise monotone map on $[0, 1]$ and the forward orbits of the critical points of f are finite (f is a Markov map), then these orbits provide a finite partition of the interval I into intervals I_k . The preimage of each I_k consists of a union of preimages each of which lies in a distinct subinterval I_j . We can therefore create k trees of intervals with $I_k = I_k^0$ placed at the root of each tree. The remainder of the tree is constructed exactly as in the case of the tent map discussed above. Repeating the argument outlined above, we can again obtain an invariant collection of graphs. The dynamics of this collection is again determined completely by the path in the tree chosen to construct the graph (which is exactly a symbolic sequence for the Markov map), and the attractor is again contained in this invariant collection (see [2] for an alternative construction).

Remark 4.3 *This argument only shows that there exists an invariant collection of continuous graphs. The contraction mapping theorems used to prove the smoothness of the invariant manifold in the case of invertible maps are more technical [28, 9, 15], but can be extended to the present case. The smoothness of the invariant manifold can be guaranteed only if the rate of contraction of f given by (3.7) does not exceed the rates of contraction of g given by (3.6). In the case when f is an expanding map, this condition is always satisfied. However, if f is smooth and noninvertible, the contraction rate at the singular points is unbounded. Orbits that return often to a neighborhood of these points will display similarly high contraction rates and the conditions for smoothness may not be satisfied, regardless of the contraction rate in (3.6). Estimating the size of the set of orbits on which such high contraction occurs is a delicate question. For a more detailed discussion see [5, 28, 12, 27].*

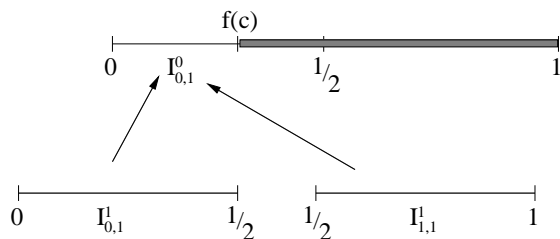


Figure 8: Constructing the first level of the tree for (2.2), with $c < 1$. The shaded parts of the interval are trimmed at this level.

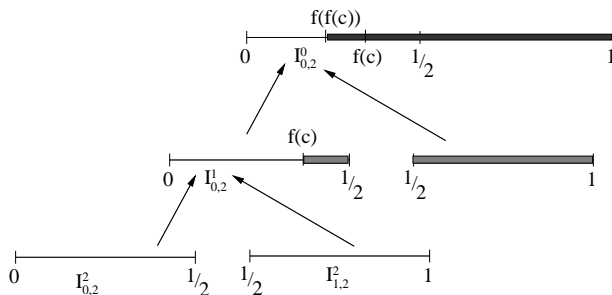


Figure 9: The second level of the tree for (2.2), with $c < 1$ with shaded parts being trimmed.

4.3 Extensions of the construction

If the orbit of the critical point is not finite, the construction becomes somewhat more involved. In this case only part of an interval that occurs in the construction of the tree may be in the range of f . When this occurs we need to “trim” away the part of the interval that is not in the range. We present two particular examples. Although the first example is trivial, it is chosen to clearly illustrate the general procedure.

Let us again consider the tent map (2.2), and let $c < 1$. Note that in this case f is not an expanding map. We again start the construction of the tree by considering the root interval $I_0^0 = [0, 1]$. However the image of the intervals $I_0^1 = [0, 1/2]$ and $I_1^1 = [1/2, 1]$ is $f(I_0^1) = f(I_1^1) = [0, f(c)]$ is not the entire interval. We therefore replace the interval $I_0^0 = [0, 1]$ with the interval $[0, f(c)]$ at this level of the construction and obtain two paths $(I_{0,1}^0, I_{0,1}^1)$ and $(I_{0,1}^0, I_{1,1}^1)$, where the second subscript denotes the level of construction (See Fig. 8).

To construct the next level of intervals, note that the interval $I_1^1 = [1/2, 1]$ has no preimage under f , so the path $(I_{0,1}^0, I_{1,1}^1)$ terminates at this point. On the other hand, the path $(I_{0,1}^0, I_{0,1}^1)$ can be extended to create the next level of paths $(I_{0,2}^0, I_{0,2}^1, I_{0,2}^2)$ and $(I_{0,2}^0, I_{0,2}^1, I_{1,2}^2)$ where $I_{0,2}^0 = [0, f(f(c))]$, $I_{0,2}^1 = [0, f(c)]$, $I_{0,2}^2 = [0, 1/2]$, and $I_{1,2}^2 = [1/2, 1]$ (see Fig. 9).

This construction can be continued indefinitely, and results in a single path $(I_{0,\infty}^0, I_{0,\infty}^1, \dots, I_{0,\infty}^n, \dots)$

with $I_{0,\infty}^n = 0$ for all n . Although this is a very indirect way to reach the conclusion that we can only construct an invariant graph over the fixed point $x = 0$, it illustrates the generally applicable procedure of trimming intervals along the branches tree.

The synchronization set in this case only contains one point with x -coordinate 0, and y -coordinate determined by the response map. The same construction for the tent map when $c > 1$ results in a number of sequences. Some of these sequences may terminate, and some may result in sequences of points rather than intervals. However, in the case of piecewise monotone maps, at least some of the sequences will consist of non-degenerate intervals [19]. Therefore, at least a portion of the synchronization set will consist of graphs of continuous curves over intervals. Unlike the case of Markov maps, in general the topology of the invariant collection of intervals is difficult to determine using this construction. Despite this, we will show in section 4.5, that we can still approximate the invariant graph with a collection of intervals.

This construction is closely related to the inverse limit construction discussed in section 3. The collection of graphs constructed using this procedure corresponds to

$$\bigcup_{x \in (X, f)} (x_0, \Phi(x)) = \bigcup_{x \in (X, f), i \in \mathbb{N}} (x_i, \Phi(x))$$

where $x = \{x_0, x_1, x_2, \dots\}$ is the inverse limit sequence described in section 4.5, and $\Phi : (X, f) \rightarrow Y$ is the invariant graph over the inverse limit discussed in the previous section. This explains our earlier claim that this graph may be viewed as the projection of the graph Φ onto the first coordinate in the inverse limit. We may also use this observation to conclude that, since the graph Φ is bounded, there exists a C such that $|\Psi_{a_j, \infty}^j(x)| < C$ for any graph in the invariant collection.

Remark 4.4 *There are several constructions of inverse limits which are pseudoarcs and therefore do not contain any intervals [14, 20]. If the bonding maps used to construct these inverse limits are used in our construction, all sequences of intervals will be degenerate, i.e. all will be sequences of points. Therefore no points of the synchronization set are contained in continuous curves. As noted, this does not happen for piecewise monotone maps.*

4.4 Connections between graphs in the invariant collections

It is apparent in Fig. 1a that the different graphs in the invariant collection are connected along the forward orbit of the critical point. In this section we show that this is true in the case of a tent map with $c = 2$, and discuss how to extend these observations.

In the construction of the tree of intervals in section 4.1, each pair of adjacent intervals shares an endpoint. Consider the sequences $\{k_n(1/2)^n\}_{n=0}^\infty$ where $k_0 = 1$ and $f(k_{n+1}(1/2)^{n+1}) = k_n(1/2)^n$. Each such sequence corresponds to one possible backward orbit of the critical point $1/2$. There are two intervals $J_{i_1}^n$ and $J_{i_2}^n$ which share $k_n(1/2)^n$ as an endpoint. Therefore there are two paths of intervals, in the tree, such that at each level

the two corresponding intervals share an endpoint. Since $k_n(1/2)^n \neq 1/2$ it follows that f is invertible along this path, except at the top level. Therefore we can take the union of the two intervals at each level to show that our construction gives a unique graph over the interval $[0, 1]$ at the 1st level of the tree. This interval is then mapped to two intervals at the 0th level of the tree which are joined at the image of the critical point, $f(1/2) = 1$.

In section 4.1 it was shown that the invariant collection of graphs Ψ^* equals the union of top level graphs $\Psi_{a_0}^*$. The argument in the previous paragraph shows that all connections among the top level graphs occur at the critical point and its images. Moreover, two graphs $\Psi_{a_0}^*$ and $\Psi_{b_0}^*$ will be connected if all pairs of intervals $J_{a_k}^k$ and $J_{b_k}^k$ share a common endpoint corresponding to an orbit that eventually lands at a critical point.

The same observation is true more generally. In the extended construction described in 4.3, the intervals in two branches in the extended tree will share a point, if and only if each pair of intervals at a certain level shares an endpoint which eventually maps to a critical point of the map.

As a simple example, consider the map

$$f(x) = \begin{cases} 2x & \text{if } x \in [0, \frac{1}{2}) \\ -x + \frac{3}{2} & \text{if } x \in [\frac{1}{2}, 1] \end{cases} \quad (4.9)$$

The tree of intervals corresponding to this equation has $k + 2$ intervals at the k th level, and hence there are only a countable number of branches. Using the argument outlined above, it is immediate that the different branches correspond to intervals that are joint alternately at $x = 1/2$ and $x = 1$. Not surprisingly, the inverse limit for this map is equivalent to the topologist's sine curve.

A question posed in [2] is whether the invariant graph can consist of a countably infinite number of curves when the driving map has positive topological entropy. The following example answers the question in the affirmative. It is a drive-response system of the form (3.4), where the drive is the logistic map $f(x) = \mu_1 x(1 - x)$ for $\mu_1 = 4$. It is well known that this drive has positive topological entropy. The response is given by the formula:

$$g(x, y) = h(x) \mu_2 x(1 - x) + (1 - h(x)) f(x), \quad (4.10)$$

and μ_2 chosen to be near 4 (for example, we use $c = 3.7$), and h is a differentiable function defined by

$$h(x) = \begin{cases} N(x_1 - x)^2 & \text{if } x \in [0, x_1) \\ 0 & \text{if } x \in [x_1, x_2], \\ N(x - x_2)^2 & \text{if } x > x_2. \end{cases} \quad (4.11)$$

where $x_1 = (1 - 1/\sqrt{2})/2$, $x_2 = (1 + 1/\sqrt{2})/2$, and $N = \frac{1}{2x_1^2}$. Note that $f^{-1}([1/2, 1]) = [x_1, x_2]$. Thus for $x \in [x_1, x_2]$, $g(x, y) = f(x)$. Thus the synchronization set is the graph of a single curve for all $x \in [1/2, 1]$. The fact that there is only a single curve propagates through all the branches of the tree structure which reach this right half of the interval $[0, 1]$, with the result that above $[0, 1/2]$, there is a countably infinite number of curves. To see

this, consider two points $\{x_0, x_1, \dots\}$ and $\{z_0, z_1, \dots\}$ in the inverse limit space for (X, f) . If $x_0 = z_0 > 1/2$, then the points correspond to the same point on the synchronization set independent of all other values in the sequence. Therefore, except for a sequence with all points less than $1/2$, all other points on the synchronization set S are determined by a finite sequence.

The number of curves above the interval $(0, 1/2)$ is countably infinite rather than finite. (The curves all intersect at 0 and $1/2$.) To show this we calculate the unique curve Γ_R of S which is a graph over the interval $(1/2, 1]$ and the unique curve Γ_0 which is a graph over $[0, 1/2]$ with a k^{th} backward orbit in $[0, x_1^{-k}]$ for all k . We use the invariance of the synchronization set; the iterate of Γ_R under the system has a portion which is a graph over $(0, 1/2)$. This is distinct from Γ_0 . As a result of this and the fact that f is one-to-one on this interval, every iterate of these two curves, restricted to $(0, 1/2)$, is a distinct curves as well. This gives a countably infinite number of distinct curves.

The previous example is carefully constructed so that many curves in the inverse limit space project onto the same curve in the original space. We conjecture that this non-generic collapse is necessary in order to have a countable number of curves when the topological entropy is positive.

4.5 Approximations of the invariant collection

In this section we show that the full invariant collection of graphs can be approximated to arbitrary accuracy by a specific finite collection of graphs when f is uniformly expanding. Therefore, even in very complex situations, the synchronization set looks like a union of curves. The argument is again presented for the case of a tent map (2.2) with $c = 2$, and can be generalized.

For an arbitrary $\epsilon > 0$, we will construct a finite set of graphs, each of which will lie within a distance ϵ of an uncountable number of graphs in the invariant collection. The union of these representative graphs provides the desired approximation.

Since f is uniformly expanding, the intervals $J_{a_n, n}^n$ at the n -th level of construction in the paths $(J_{a_0, n}^0, J_{a_1, n}^1, \dots, J_{a_n, n}^n, \dots)$ have length smaller than $(1/2)^n$, and there exists an N such that $(1/2)^N < \epsilon$. Fix the finite sequence $\{a_0, \dots, a_N\}^1$.

As noted earlier, all graphs in the invariant collection are bounded by some $C > 0$. Let M be such that $Cc_1^M < \epsilon$ where c_1 is defined in (3.6). Select a fixed sequence $\{a_0, \dots, a_N, \dots, a_{N+M}\}$ and continue the construction that was terminated at the level N to the level $N+M$, to obtain the paths $(J_{a_0, N+M}^0, \dots, J_{a_N, N+M}^N, \dots, J_{a_{N+M}, N+M}^{N+M})$. Consider the functions $\tilde{\Psi}_{a_{N+M}, N+M}^{N+M} = 0$ defined over each interval at this level, and consider the M -th forward image of graph $(\tilde{\Psi}_{a_{N+M}, N+M}^{N+M})$. This is the graph of a function $\tilde{\Psi}_{a_N, N}^N : I_{a_N, N+M}^N \rightarrow Y$. By construction

$$\sup_{x \in I_{a_N, \infty}^N} |\tilde{\Psi}_{a_N, N}^N(x) - \Psi_b^{N^*}(x)| < Cc_1^M < \epsilon,$$

¹In the case of the tent map with $c = 2$, this first step is not necessary, however it becomes essential when the orbit of the critical point is not finite.

where $\Psi_b^{N,*}$ is the N -th graph of *any* sequence Ψ_b^* in the invariant collection such that $\{b_0, \dots, b_{N+M}\} = \{a_0, \dots, a_{N+M}\}$ where $\{a_0, \dots, a_{N+M}\}$ is the sequence fixed in the previous step. Therefore $\tilde{\Psi}_{a_N, N}^N(x)$ gives an ϵ -approximation of any graph in the invariant collection corresponding to a sequence that starts with $\{a_0, \dots, a_{N+M}\}$. Taking the finite union of graphs corresponding to all possible starting segments $\{a_0, \dots, a_{N+M}\}$ gives an ϵ -approximation of the entire invariant collection.

This argument can be extended to the case of nonuniformly expanding maps, and maps that are expanding on average by modifying the choice of μ . Therefore, regardless of the topological complexity of the invariant collection, it can always be approximated by nearly invariant collection consisting of finitely many graphs.

Remark 4.5 *In Fig. 1a and b, we took $c = 1.9999$, since binary arithmetic makes numerical analysis of the case $c = 2$ difficult. The results of this section show that the invariant collections of graphs in the two cases will be close. This follows from the facts that only a finite number of iterates are necessary to construct an arbitrarily good approximation of the collection, and the dynamics depends continuously (even differentiably) on the parameter c .*

4.6 A note on detection methods

In [27] it was shown that methods that rely on continuity for the detection of synchronous states typically fail in the case of noninvertible systems. A typical example is given by the ϵ - δ method where one chooses a ball $B(x, \delta)$ around a reference point x , and iterates the driving system in (3.4) until the orbit falls within $B(x, \delta)$ a large number of times. To each point $x_{a_i} \in B(x, \delta)$ on the orbit, there corresponds a point $y_{a_i} \in Y$ such that (x_{a_i}, y_{a_i}) lies on the attractor of (3.4). Let ϵ be the radius of the smallest ball in y containing all y_{a_i} . If the attractor lies in a smooth or Lipschitz manifold, then ϵ decreases linearly with δ . If f is noninvertible, the attractor will be in a collection of graphs. In this case ϵ will typically not decay with δ because nearby points in $B(x, \delta)$ may have different histories, and the corresponding points y_i may not lie on the same graph.

In [13] it was argued that a modification of the method can be applied to detect synchronization in the case f is noninvertible. Let x^* and z^* be two points on the orbit of x_0 and z_0 on the attractor, under the evolution of the driving system. Consider the subsets of the orbits of x_0 and z_0 defined by $\mathbf{x}_p^* = (x_n, f(x_n), \dots, f^{p-1}(x_n))$ where x_n is some point on the orbit of x_0 satisfying $f^{p-1}(x_n) = x^*$, and $\mathbf{z}_p^* = (z_m, f(z_m), \dots, f^{p-1}(z_m) = z^*)$ (note that m does not have to equal n). The point z^* is said to be δ^p close to x^* if $|f^k(x_n) - f^k(z_m)| < \delta$ for all $0 < k < p - 1$, so that entire portions of the orbits of x_0 and z_0 consisting of p points are required to be δ -close. This notion of distance and the associated ϵ - δ^p test can be used to detect synchrony even when f is noninvertible.

The effectiveness of this method can be explained using the ideas described in the previous section. We again consider the tent map (2.2) with $c = 2$, as an illustrative case. Two points x^* and z^* are δ^p close, if their partial orbits $\mathbf{x}_p^* = (x_n, f(x_n), \dots, f^{p-1}(x_n) = x^*)$ and $\mathbf{z}_p^* = (z_m, f(z_m), \dots, f^{p-1}(z_m) = z^*)$ constitute the head of two closeby elements of

the inverse limit space. This means that most likely $f^k(z_m), f^k(x_n) \in J_a^{p-k-1}$ for some sequence a and intervals J_a^0, \dots, J_a^{p-1} in the tree defined in Section 4.1. Since only the head of the two symbolic sequences corresponding to x^* and z^* are required to match, their images do not necessarily lie on the same graph. However we know that the points $\Psi_a^0(x^*)$ and $\Psi_b^0(z^*)$ in the invariant collection correspond to two sequences a and b such that $\{a_0, \dots, a_{p-1}\} = \{b_0, \dots, b_{p-1}\}$. Therefore

$$\begin{aligned} |\Psi_a^0(x^*) - \Psi_b^0(z^*)| &\leq (|\Psi_a^0(x^*) - \Psi_a^0(z^*)| + |\Psi_a^0(z^*) - \Psi_b^0(z^*)|) \\ &\leq \epsilon(\delta, x^*) + c_2^{p-1} |\Psi_a^{p-1}(z_m) - \Psi_b^{p-1}(z_m)| \\ &\leq \epsilon(\delta, x^*) + c_2^{p-1} C \end{aligned} \quad (4.12)$$

where c_2 is defined in (3.6), C is the size of the attractor in the vertical direction, and $\epsilon(\delta, x^*) = \max_{z \in B(x^*, \delta) \cap J_a^0} |\Psi_a^0(z) - \Psi_a^0(x^*)|$. As in the invertible case, $\epsilon(\delta, x^*)$ will decay to 0, and it will decay linearly if $\Psi^0 - a(x^*)$ is differentiable or Lipschitz at x^* .

Therefore, if the attractor of the system is contained in an invariant collection of continuous graphs, the $\epsilon - \delta^p$ method can be used to analyze the regularity of the graphs in this collection. Increasing p decreases $c_2^{p-1}C$, and therefore the resolution of the method.

5 Bifurcation to a noninvertible drive

An example in Section 2.3 illustrated how the invariant graph either developed hooks (Fig. 10b), or loops (Fig. 10d) as the map defining the driving system changes from being invertible to noninvertible. In this section we provide a heuristic argument why typically near the bifurcation, the invariant graph is close to a smooth manifold without self intersecting loops.

Consider a system $(x, y) \mapsto (f(x), g(f(x), y))$ with $y \in \mathbf{R}$. The idea of the argument is illustrated in Fig. 10. Assume that we have a piece of a graph $\phi(x)$. Choose 4 points $x_1 < x_2 < x_3 < x_4$ in the domain of the graph. We assume that the response system contracts the y direction, and that ϕ does not change the ordering of the points, so that $\phi(x_1) < \phi(x_2) < \phi(x_3) < \phi(x_4)$. Also assume that $f : \mathbf{R} \rightarrow \mathbf{R}$ has the shape of the cubic with two critical points at x_2 and x_3 (see Fig. 5b), so that $f(x_1) < f(x_3) < f(x_2) < f(x_4)$. If ϕ is monotone between x_1 and x_4 (as in Fig. 10a), it is easy to see that the image of the graph of ϕ will be nonintersecting (as in Fig. 10b). On the other hand if ϕ has a critical point between x_2 and x_3 (see Fig. 10c), a loop will be formed under one iterate (shown in Fig. 10d).

More formally the synchronization set is contained in the invariant graph of a function ϕ which satisfies $\phi(f(x)) = g(f(x), \phi(x))$. Assume that the f is a monotone increasing function such that $f'(x_*) = 0$ (see the middle graph in Fig. 5a). Then $f'(x)$ has the same sign for all $x \neq x_*$. The tangent of S is such that:

$$\phi'(f(x))f'(x) = D_1g(f(x), \phi(x))f'(x) + D_2g(f(x), \phi(x))\phi'(x).$$

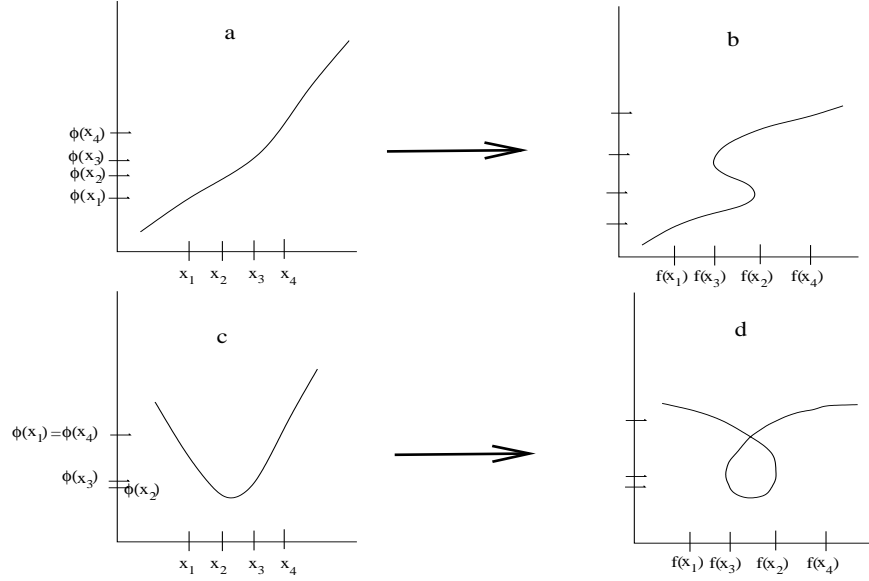


Figure 10: a. When ϕ is a monotone graph of a function near x , then b. the synchronization set near $f(x)$ becomes multivalued without containing self intersections. c. If the synchronization set has a critical point corresponding with a critical point x of f , then d. the synchronization set contains point of self-intersection, or loops, immediately upon becoming multivalued.

Whenever $\phi'(x_*)D_2g(f(x_*), \phi(x_*)) \neq 0$, $\phi'(f(x_*))$ limits to a well-defined vertical tangent ∞ or $-\infty$, corresponding to the sign of $f'(x)$ for $x \neq x_*$. Therefore by the implicit function theorem, the synchronization set can be written as the graph of a smooth function $x = \eta(y)$ from Y to X . For nearby parameter values, this smoothness may not persist, as the points at which $\eta'(y) = 0$ may be dense, depending on the orbit of the critical point of f . However, since we have assumed that (3.6) holds, the contraction will make the large iterates of this “wrinkle” very small, so that the the set will still be approximated well by a smooth manifold. Thus the only possible self intersections will only be visible under very high magnification². However, if $\phi'(x)D_2g(f(x), \phi(x))$ changes sign at x_* , then the lefthand and righthand limits of $\phi'(f(x))$ are both infinite but disagree in sign, implying a cusp.

In our specific example, $(u, \phi(u))$ maps to $(f(u), c\phi(u) + g(f(u)))$. The function f is increasing and has a critical point at $s = 0$, when $u = \rho, v < \alpha$. Thus the synchronization set has a cusp exactly when it has a minimum (or maximum) at $u = \rho$. For ρ near $1/2$, this can be achieved by varying the coupling parameter c .

²The closer we are to the bifurcation the larger the magnification necessary to detect these potential loops.

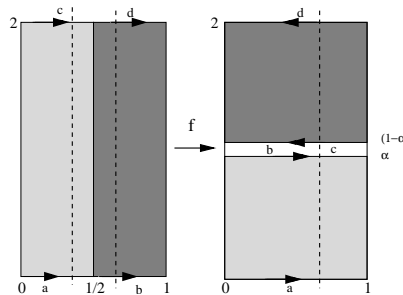


Figure 11: A schematic of baker's map which can be thought of as an extension of the tent map. The two dotted lines on the left are preimages of the dotted line on right, and project to a point under ϕ .

6 An alternative construction

In section 4.1 we illustrated the construction of an invariant collection of continuous graphs for system (3.4), but did not address the smoothness of the graphs in the collection. In this section we show how to introduce an invariant map with an invariant foliation which can be used to address this question directly, and use a similar idea to explain the structure of attractors of the systems introduced in 2.2.

As a simple example of the construction once again consider the tent map (2.2). A map $g : Y \rightarrow Y$ is a factor of a map $f : X \rightarrow X$ if there exists a map $\phi : X \rightarrow Y$ such that $\phi(f(x)) = g(\phi(x))$. It is easy to see that the tent map is a factor of the baker's map

$$x'_1 = F_1(x_1) = \begin{cases} 2x_1 & x_1 < 1/2 \\ -2x_1 + 1/2 & x_1 \geq 1/2 \end{cases} \quad (6.13)$$

$$x'_2 = F_2(x_1, x_2) = \begin{cases} \alpha x_2 & x_1 < 1/2 \\ \alpha x_2 + (2 - \alpha) & x_1 \geq 1/2 \end{cases} \quad (6.14)$$

where $\alpha < 1$. In this case $\phi : [0, 1] \times [0, 2] \rightarrow [0, 1]$ is the projection onto the x -axis, so that $\phi(x, y) = x$ is the projection onto the x -axis (see Fig. 11). Note that by choosing α close to 1, the amount of contraction in the x_2 direction can be made arbitrarily small.

This map is not invertible on the entire unit square, since the inverse is not defined outside of the shaded areas of Fig. 11. Since we are only interested in the invariant graph over the attractor, we can either extend the map arbitrarily to an invertible map of the plane, or restrict the map to its attractor. The map is discontinuous, but only along the line $x_1 = 1/2$.

Using a similar construction, we can extend any map $f : [0, 1] \rightarrow [0, 1]$ with finitely many critical points, to an invertible map of a rectangle $[0, 1] \times [0, N]$ where N is the number of critical points. An example is given in Fig. 12.

We can therefore associate a system

$$x_{n+1} = F(x_n) \quad y_{n+1} = G(\phi(x_n), y_n) \quad (6.15)$$

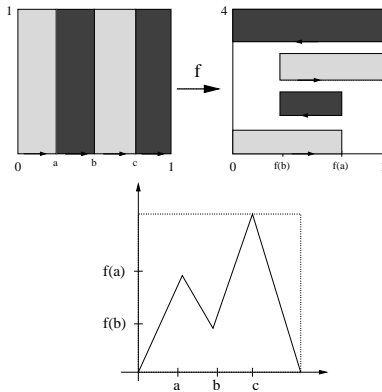


Figure 12: An extension of a multimodal map. The graph of the factor map is below the extension. Note that the vertical direction in the range of f has been shortened.

with system (3.4) where F is invertible. If A is the attractor of (6.15), then $\tilde{\phi}(A)$ is the attractor of (3.4), where $\tilde{\phi}$ is the projection to the first and third coordinates $\tilde{\phi}(x_1, x_2, y) = (x_1, y)$.

We can use this extension to discuss the smoothness of the graph over the attractor of the driving map. Since the extended map is invertible the usual theory of invariant manifolds can be applied away from the orbits of points of discontinuity – corresponding to the orbits of the critical points of the map – which are expected to form a small set. The graph over attractor A of (6.15) is the restriction of the invariant manifold to this set. Since the projection $\tilde{\phi}$ is smooth, any existing curves in A will be projected smoothly to curves in $\tilde{\phi}(A)$. The contraction in the map can be made arbitrarily small, so that the smoothness of this manifold depends only on the contraction of the noninvertible map used in the construction.

We use a similar argument to explain the structure of the synchronization set observed in section 2.2, where the Lorenz system was used as a drive. Let f denote the Poincaré map defined on the section $z = 27, |x| < 8$. There is a stable invariant foliation in the vicinity of the attractor in this Poincaré section [30]. If we denote the projection along this stable foliation by ϕ , the map $\tilde{f}(x) = f(\phi(x))$ is a noninvertible map of the interval which is discontinuous at a single point, and monotone away from this point. If we consider \tilde{f} as the driving map in a drive-response system of type (3.4), the theory discussed in section 3 can be applied to construct a tree of intervals and an invariant collection of graphs with a transversal Cantor-like structure³. Since the only critical point of \tilde{f} is the point of discontinuity, the different graphs in the collection will not be connected. A particular projection of this invariant collection of graphs is what is observed in Fig. 2.

We emphasize that in this situation there exists an invariant graph $\Psi : \mathbf{R}^3 \rightarrow \mathbf{R}$. The

³Since the map \tilde{f} is not uniformly expanding, the arguments about the smoothness of the graphs in the collection require delicate estimates.

attractor of the full 4-dimensional system lies in this invariant graph. What is observed in Fig. 2 is a section of the attractor in this invariant graph. Since the dissipation of the Poincaré map in this case is very strong, this section is very thin in the direction of the stable foliation. The section is therefore very close to its projection under ϕ , and hence we observe an object close to one which can be described using the arguments of section 3. A similar argument explains the structure of the attractor in the case of the Rössler system, although, we are not aware of a proof of the existence of an invariant foliation in this case.

We expect that strongly dissipative systems will result in attractors with similar structures when used as drives in this type of drive-response systems. In such cases the structure in the strongly contracted directions may, in a sense, be resolved in the response system.

7 Conclusion

We have shown that the attractors of certain drive-response systems in general lie on an invariant collection of graphs of functions from the phase space of the driving system to the phase space of the response. Although this collection may have a very complex geometry, under certain condition it can be approximated by a finite collection of nearly invariant graphs. This explains the occurrence of striated structures frequently observed in in numerical and physical experiments [5, 8].

It is likely that the attractors in many dissipative systems have strong stable foliations along which they can be projected to lower dimensional, noninvertible systems [30, 31]. Moreover, noninvertibility is a natural occurrence in many numerical and physical experiments. The arguments given in this paper are applicable in many such cases, and can show that certain response systems could provide an effective way of studying the structure of their attractor.

We have not addressed several interesting questions: It is clear from Fig. 1 that the different graphs in the invariant collection will intersect at various points. Where do these intersections occur? It would also be interesting to estimate a dimension of the attractor as a function of the coupling strength.

A Γ_a is a contraction

Let Ψ_a and Φ_a be two sequences of graphs in G_a . Then

$$\begin{aligned}
d_i(\Gamma_{a_i}(\Psi_{a_i}^i), \Gamma_{a_i}(\Phi_{a_i}^i)) &= \sup_{x \in J_{a_i}^i} |\Gamma_{a_i}(\Psi_{a_i}^i)(x) - \Gamma_{a_i}(\Phi_{a_i}^i)(x)| \\
&= \sup_{x \in J_{a_i}^i} |g(f_{a_{i+1}}(x), \Psi_{a_{i+1}}^{i+1}(f_{a_{i+1}}^{-1}(x))) - g(f_{a_{i+1}}(x), \Phi_{a_{i+1}}^{i+1}(f_{a_{i+1}}^{-1}(x)))| \\
&< e^\lambda \sup_{x \in J_{a_{i+1}}^{i+1}} |\Psi_{a_{i+1}}^{i+1}(x) - \Phi_{a_{i+1}}^{i+1}(x)| \\
&= e^\lambda d_{i+1}(\Psi_{a_{i+1}}^{i+1}, \Phi_{a_{i+1}}^{i+1}) \tag{A.16}
\end{aligned}$$

where the second to last inequality follows from (3.6).

Inequality (A.16) implies directly that

$$\begin{aligned}
\bar{d}_\eta(\Gamma_a(\Psi_a), \Gamma_a(\Phi_a)) &\leq \sum_{i=0}^{\infty} e^\lambda \frac{d_{i+1}(\Psi_{a_{i+1}}^{i+1}, \Phi_{a_{i+1}}^{i+1})}{e^{\eta i}} \\
&= e^{\lambda+\eta} \sum_{i=0}^{\infty} \frac{d_{i+1}(\Psi_{a_{i+1}}^{i+1}, \Phi_{a_{i+1}}^{i+1})}{e^{\eta(i+1)}} \\
&\leq e^{\lambda+\eta} \sum_{i=0}^{\infty} \frac{d_i(\Psi_{a_i}^i, \Phi_{a_i}^i)}{e^{\eta i}} \\
&= e^{\lambda+\eta} \bar{d}_\eta(\Psi_a, \Phi_a),
\end{aligned} \tag{A.17}$$

and choosing η so that $\lambda + \eta < 1$ ensures that Γ_a is a contraction on G_a . It follows from the contraction mapping theorem that there exists an invariant sequence of graphs $\Psi_a^* \in G_a$.

Acknowledgments

K.J. was partially supported by grant NSF-0244529. E.S. was partially supported by George Mason University Provost's Office summer research funding.

References

- [1] V. Afraimovich, J.-R. Chazottes, and A. Cordonet. Synchronization in directionally coupled systems: Some rigorous results. *Discrete and Continuous Dynamical Systems B*, 1:421–442, 2001.
- [2] V. Afraimovich, A. Cordonet, and N. Rulkov. Generalized synchronization of chaos in non-invertible maps. *Phys. Rev. E*, 66:016208, 2002.
- [3] M. Barge, K. Brucks, and B. Diamond. Self-similarity in inverse limit spaces of the tent family. *Proc. Amer. Math. Soc.*, 124(11):3563–3570, 1996.
- [4] M. Barge and W. T. Ingram. Inverse limits on $[0, 1]$ using logistic bonding maps. *Topology Appl.*, 72(2):159–172, 1996.
- [5] E. Barreto, K. Josić, C. J. Morales, E. Sander, and P. So. The geometry of chaos synchronization. *Chaos*, 13(1):151–164, 2003.
- [6] S. Boccaletti, J. Kurths, G. Osipov, D. L. Valladares, and C. S. Zhou. The synchronization of chaotic systems. *Phys. Rep.*, 366(1-2):1–101, 2002.
- [7] S. Boccaletti, L. Pecora, and A. Pelaez. Unifying framework for synchronization of coupled dynamical systems. *Phys. Rev. E*, 63:066219, 2001.

- [8] J. Chubb, E. Barreto, P. So, and B. Gluckman. The breakdown of synchronization in systems of nonidentical chaotic oscillators: Theory and experiment. *International Journal of Bifurcations and Chaos*, 11:2705–2713, 2001.
- [9] N. Fenichel. Persistence and smoothness of invariant manifolds for flows. *Indiana Univ. Math. J.*, 21:193–226, 1971/1972.
- [10] C. E. Frouzakis, R. A. Adomaitis, I. G. Kevrekidis, M. P. Golden, and B. E. Ydstie. The structure of basin boundaries in a simple adaptive control system. In *Chaotic dynamics (Patras, 1991)*, volume 298 of *NATO Adv. Sci. Inst. Ser. B Phys.*, pages 195–210. Plenum, New York, 1992.
- [11] J. Guckenheimer and R. F. Williams. Structural stability of Lorenz attractors. *Inst. Hautes Études Sci. Publ. Math.*, (50):59–72, 1979.
- [12] D. Hadjiloucas, M. J. Nicol, and C. P. Walkden. Regularity of invariant graphs over hyperbolic systems. *Ergodic Theory Dynam. Systems*, 22(2):469–482, 2002.
- [13] D. He, Z. Zheng, and L. Stone. Detecting generalized synchrony: An improved approach. *Phys. Rev. E*, 67:026223, 2003.
- [14] G. W. Henderson. The pseudo-arc as an inverse limit with one binding map. *Duke Math. J.*, 31:421–425, 1964.
- [15] M. W. Hirsch, C. C. Pugh, and M. Shub. *Invariant manifolds, Lecture Notes in Mathematics, Vol. 583*. Springer-Verlag, Berlin, 1977.
- [16] K. Josić. Synchronization of chaotic systems and invariant manifolds. *Nonlinearity*, 13(4):1321–1336, 2000.
- [17] E. Lorenz. Deterministic nonperiodic flows. *J. of Atmospheric Sciences*, 20:130–141, 1963.
- [18] E. N. Lorenz. Computational chaos—a prelude to computational instability. *Phys. D*, 35(3):299–317, 1989.
- [19] W. S. Mahavier. Arcs in inverse limits on $[0, 1]$ with only one bonding map. *Proc. Amer. Math. Soc.*, 21:587–590, 1969.
- [20] P. Minc and W. R. R. Transue. A transitive map on $[0, 1]$ whose inverse limit is the pseudoarc. *Proc. Amer. Math. Soc.*, 111(4):1165–1170, 1991.
- [21] S. B. Nadler, Jr. *Continuum theory, An introduction*, volume 158 of *Monographs and Textbooks in Pure and Applied Mathematics*. Marcel Dekker Inc., New York, 1992.
- [22] A. Pikovsky, M. Rosenblum, and J. Kurths. *Synchronization: A Universal Concept in Nonlinear Science*. Cambridge University Press, Cambridge, 2003.

- [23] N. Rulkov and V. Afraimovich. Detectability of non-differentiable generalized synchrony. *Physical Review E*, 61:066218–1–066218–8, 2003.
- [24] N. Rulkov, V. Afraimovich, L. Lewis, J.-R. Chazottes, and A. Cordonet. Multivalued mappings in generalized chaos synchronization. *Physical Review E*, 64:016217, 2001.
- [25] N. F. Rulkov, M. Suschik, L. S. Tsimring, and H. Abarbanel. Generalized synchronization of chaos in directionally coupled chaotic systems. *Phys. Rev. E*, 51(2):980–994, 1995.
- [26] E. Sander, E. Barreto, K. Josic, and P. So. Synchronization sets in drive-response systems. In *SIAM DSWeb Online Picture Gallery*. <http://www.dynamicalsystems.org/pi/sm/detail?item=35>, 2003.
- [27] P. So, E. Barreto, K. Josić, E. Sander, and S. J. Schiff. Limits to the experimental detection of nonlinear synchrony. *Phys. Rev. E*, 65:046225, 2001.
- [28] J. Stark. Regularity of invariant graphs for forced systems. *Ergodic Theory Dynam. Systems*, 19(1):155–199, 1999.
- [29] S. Strogatz. *Sync: The Emerging Science of Spontaneous Order*. Hyperion, New York, 2003.
- [30] W. Tucker. A rigorous ODE solver and Smale’s 14th problem. *Found. Comput. Math.*, 2(1):53–117, 2002.
- [31] R. F. Williams. One-dimensional non-wandering sets. *Topology*, 6:473–487, 1967.